M. Zaky

M. Khater

H. Yasin

S. S. Shokralla

J. Electrical Systems 4-1 (2008): 106-125

Regular paper

A Very Low-Speed Sensorless Induction Motor Drive with Online Stator Resistance identification scheme

Recently, speed sensorless control of induction motor drives received great attention to avoid the different problems associated with direct speed sensors. However, low speed operation with robustness against parameter variations remains an area of research for sensorless systems. Stator resistance is of greatest importance for good operation of speed sensorless systems in low speed region. In this paper, a sliding mode current observer for an induction motor is presented. An estimation algorithm based on this observer in conjunction with Popov's hyper-stability theory is proposed to calculate the speed and stator resistance independently. The proposed speed observer with parallel stator resistance identification is firstly verified by simulation. Experimental results are included as well to demonstrate the good performance of the proposed observer and estimation algorithms at low speed.

Keywords: Sliding Mode Observer (SMO), Speed Sensorless, Popov's stability, and stator resistance

1. INTRODUCTION

Several methods have been recently proposed for speed estimation of sensorless induction motor drives. A comprehensive study of the different speed estimation techniques and their specific merits and demerits as well as their feasibility for estimating the rotor speed are presented and compared in [1]. They can be classified into two major categories. The first one includes the techniques that estimate the rotor speed based on non-ideal phenomena such as rotor slot harmonic and signal injection methods. Such methods require spectrum analysis, which besides being time consuming procedures; they allow a narrow band of speed control, while the second category relies on utilization of an induction motor model. Although model-based methods of speed estimation are characterized by their simplicity, one of the problems associated with them is their sensitivity to parameter variations. Stator resistance plays an important role and its value has to be known with good precision in order to obtain an accurate estimation of the rotor speed in the low speed region [2].

The interest in stator resistance adaptation appeared recently, with the advances of speed sensorless systems and received more attention with the introduction of direct torque control (DTC) technique. An accurate value of the stator resistance is of crucial importance for correct operation of a sensorless drive in the low speed region, since any mismatch between the actual value and the set value used within the model of speed estimation may lead not only to a substantial speed estimation error but to instability as well [3, 4]. Therefore, there is a great interest in the research community to develop online stator resistance identification schemes for accurate speed estimation in the low speed region. The available online stator resistance identification schemes can be classified into a couple of distinct categories. All these methods rely on stator current measurement and chiefly require information regarding stator voltages as well [5-10]. The most famous methods include different types of estimators which often use an adaptive mechanism to update the value of stator resistance [6-10]. The stator resistance is determined in [6] by using a reactive power based model reference adaptive system (MRAS). The reactive power relies on the accuracy of other parameters such as leakage inductance and rotor resistance which

Electrical Engineering Dept., Faculty of Engineering, Minoufiya University, Shebin El-Kom, Egypt
E-mail: m_s_zaky@yahoo.com

are not necessarily constant and the result is prone to error. Adaptive full-order flux observers (AFFO) for estimating the speed and stator resistance are developed using Popov's and Lyapunov stability criteria [7, 8]. While these schemes are not computationally intensive, an AFFO with a non-zero gain matrix may become unstable. Model reference adaptive system for estimating the speed and stator resistance is developed using Popov's stability criterion [9, 10]. In such methods, the stator resistance adaptation mechanism is determined with the difference between the measured and observed stator currents.

This paper presents a speed estimation algorithm based on a sliding mode current observer which combines variable structure control, Lyapunov stability and Popov's hyper-stability theories. Since a speed estimation algorithm should be insensitive to parameter variations, especially stator resistance for low and zero speed operation; a stator resistance identification scheme based on the same theories is also developed and used in parallel with the speed estimator. Simulation and experimental results are presented at different operating conditions to demonstrate the effectiveness of the proposed estimation algorithms.

2. SPEED AND STATOR RESISTANCE ESTIMATION PROCEDURE

The proposed parallel rotor speed and stator resistance estimation schemes are designed based on the concept of hyper-stability. This foremost needs the knowledge of the observer construction which is used for speed estimation.

2.1. CONSTRUCTION OF SLIDING MODE OBSERVER

The induction motor can be represented by its dynamic model expressed in the stationary reference frame in terms of the stator current and rotor flux by the following state equation;

$$\frac{d}{dt}\begin{bmatrix} i_s^s \\ \lambda_r^s \end{bmatrix} = \begin{bmatrix} A_{11} & A_{12} \\ A_{21} & A_{22} \end{bmatrix}\begin{bmatrix} i_s^s \\ \lambda_r^s \end{bmatrix} + \begin{bmatrix} b_1 \\ 0 \end{bmatrix}\begin{bmatrix} v_s^s \end{bmatrix} = Ax + Bv_s \tag{1}$$

where A_{11}, A_{12}, A_{21}, A_{22} and b_1 are given in the appendix.

With reference to the introduced mathematical model and considering the stator currents as the system outputs, the SMO can be constructed as:

$$p\hat{i}_s^s = \hat{A}_{11}\hat{i}_s^s + \hat{A}_{12}\hat{\lambda}_r^s + b_1 v_s + K\,\mathrm{sgn}\left(\hat{i}_s^s - i_s^s\right) \tag{2}$$

$$p\hat{\lambda}_r^s = A_{21}\hat{i}_s^s + \hat{A}_{22}\hat{\lambda}_r^s \tag{3}$$

where K is the switching gain.

The error equation which takes into account parameter variation can be expressed, by subtracting Eqn. (1) from Eqn. (2), as follows

$$\frac{de_i}{dt} = A_{11}e_i + A_{12}e_\lambda + \Delta A_{11}\hat{i}_s^s + \Delta A_{12}\hat{\lambda}_r^s + K\,\mathrm{sgn}\left(\hat{i}_s^s - i_s^s\right) \tag{4}$$

where;

$$e_i = \hat{i}_s^s - i_s^s\ ,\ \ e_\lambda = \hat{\lambda}_r^s - \lambda_r^s \ \text{ and } \ \Delta A = \begin{bmatrix} \Delta A_{11} & \Delta A_{12} \\ \Delta A_{21} & \Delta A_{22} \end{bmatrix}$$

The sliding mode surface S is constructed as:

$$S(t) = e_i = \hat{i}_s^s - i_s^s = 0 \tag{5}$$

whereas, the sliding mode switching function is defined as:

$$\text{sgn}(S) = \begin{cases} 1, & \text{if } S \geq 0 \\ -1, & \text{if } S < 0 \end{cases} \tag{6}$$

If the rotor speed and stator resistance are considered as variable parameters, assuming no other parameter variations, the matrix ΔA is expressed as follows:

$$\Delta a_{11} = \frac{-\Delta R_s I}{\sigma L_s},\ \Delta a_{12} = \frac{-\Delta \omega_r J}{\varepsilon},\ \Delta a_{21} = 0,\ \Delta a_{22} = \Delta \omega_r J$$

The sliding mode occurs when the following sliding condition is satisfied;

$$e_i^T \cdot \dot{e}_i < 0 \tag{7}$$

2.2. Characteristics of Sliding Mode Observer on Sliding Surface

When the estimation error trajectory reaches the sliding surface, i.e., $S = 0$ then, from Eqn. (5), it is obvious that the observed currents will converge to the actual ones, i.e., $\hat{i}_s^s = i_s^s$. It is important to point out that this sliding surface equation is selected to guarantee that, on the sliding surface, the observer will not be affected by any system parameter or any disturbance. This means that the current observer is invariant.

According to the equivalent control concept, assuming the observed currents $\hat{i}_s^s$ match the actual currents i_s^s in the steady-state, then Eqn. (7) becomes

$$e_i^T = \dot{e}_i = 0 \tag{8}$$

from which, the error equation becomes

$$0 = a_{12} e_\lambda + \Delta a_{11} \hat{i}_s^s + \Delta a_{12} \hat{\lambda}_r^s - L \tag{9}$$

The estimation algorithm of the stator currents is constructed by a closed loop observer, as in Eqn. (2), whereas the estimation of rotor fluxes is carried out by an open loop represented by Eqn. (3) without the flux error. Therefore, the real and estimated rotor fluxes are assumed the same $\hat{\lambda}_r^s = \lambda_r^s$; thus the error equation becomes as follows

$$0 = \Delta a_{11} \hat{i}_s^s + \Delta a_{12} \hat{\lambda}_r^s - L \tag{10}$$

2.3. Stability of the Identification System

Popov's hyper-stability theory is well known as stability criterion for nonlinear feedback systems. This theory is applied here to examine stability of the proposed identification system. This requires that the error system and the feedback system are derived so that the theory could be applied.

In the sliding mode observer, using a speed identification error $\Delta\omega_r = \hat{\omega}_r - \omega_r$, a stator resistance identification error $\Delta R_s = \hat{R}_s - R_s$ and an error signal $L = -K\ \text{sgn}\left(\hat{i}_s^s - i_s^s\right)$, the error system from Eqn. (10) is written as

$$L = \Delta a_{11} \hat{i}_s^s + \Delta a_{12} \hat{\lambda}_r^s \tag{11}$$

Substitution of Δa_{11} and Δa_{12} in Eqn. (11) yields

$$L = -\frac{\Delta R_s}{\sigma L_s}\hat{i}_s^s - \frac{\Delta\omega_r J}{\varepsilon}\hat{\lambda}_r^s = -z_1\Delta R_s - z_2\Delta\omega_r \tag{12}$$

where

$$z_1 = \left(\frac{1}{\sigma L_s}\right)\hat{i}_s^s \tag{13}$$

$$z_2 = \left(\frac{J}{\varepsilon}\right)\hat{\lambda}_r^s \tag{14}$$

The Popov's integral inequality of Eqn. (11) is written as follows [10]:

$$S = \int_0^{t_0} L^T W dt \geq -\gamma^2,\ \gamma = \text{ const.} \tag{15}$$

where L^T is the input vector and $W = -z_1\Delta R_s - z_2\Delta\omega_r$, which represents the nonlinear block, is the output vector of the feedback block, and γ is a finite positive constant which does not depend on t_0.

$$S = \int_0^{t_0} L^T W dt = \int_0^{t_0} L^T\left(-z_1\Delta R_s - z_2\Delta\omega_r\right)dt \tag{16}$$

Substitution of Eqns. (13) and (14) yields

$$S = \int_0^{t_0} L^T W dt = \int_0^{t_0}\left(\frac{-L^T\Delta R_s}{\sigma L_s}\hat{i}_s^s - \frac{L^T\Delta\omega_r J}{\varepsilon}\hat{\lambda}_r^s\right)dt \tag{17}$$

$$= \int_0^{t_0}\left(\frac{-L^T\Delta R_s}{\sigma L_s}\hat{i}_s^s\right)dt + \int_0^{t_0}\left(\frac{-L^T\Delta\omega_r J}{\varepsilon}\hat{\lambda}_r^s\right)dt$$

$$S = S_1 + S_2 \geq -\gamma^2 \tag{18}$$

$$S_1 = \int_0^{t_0}\left(-\frac{L^T\Delta R_s}{\sigma L_s}\hat{i}_s^s\right)dt \geq -\gamma_1^2 \tag{19}$$

$$S_2 = \int_0^{t_0}\left(\frac{-L^T\Delta\omega_r J}{\varepsilon}\hat{\lambda}_r^s\right)dt \geq -\gamma_2^2 \tag{20}$$

The validity of Eqn. (18) can be verified by means of the inequalities expressed by Eqns. (19) and (20), provided that the estimate of rotor speed and stator resistance can be obtained by Eqns. (21) and (22), respectively:

$$\hat{\omega}_r = K_\omega\int L^T J\hat{\lambda}_r dt \tag{21}$$

$$\hat{R}_s = K_R\int L^T i_s^s dt \tag{22}$$

where K_ω and K_R are adaptive gains.

It is verified that the Popov's inequality of Eqn. (13) is satisfied if the estimate of the stator resistance is chosen to be a linear function of an inner product of the current estimate $\hat{i}_s^s$ and the error signal *L,* and the estimate of the rotor speed is chosen to be a linear function of an inner product of the flux estimate $\hat{\lambda}_r$ and the error signal.

An identification system for speed and stator resistance is shown in Fig. 1, which is constructed from a linear time-invariant forward block and a nonlinear time-varying feedback block. The system is hyper-stable if the forward block is positive real and the input and output of the nonlinear feedback block satisfies Popov's integral inequality. Figure 2 illustrates the block diagram of parallel speed and stator resistance estimation algorithms based on a combination of SMO and Popov's hyper-stability theory.

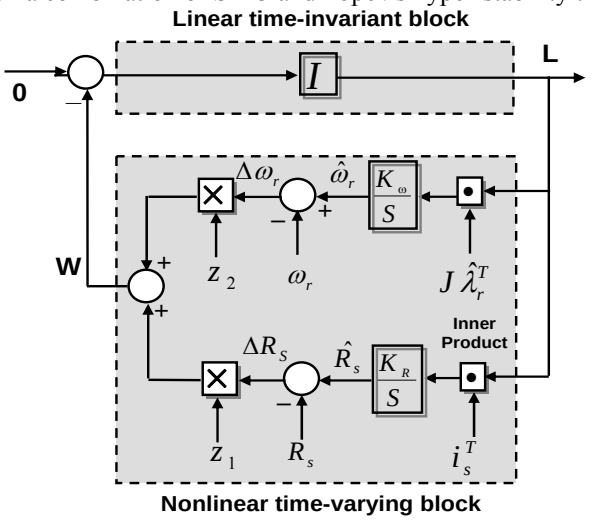

Fig. 1 Identification system for speed and stator resistance

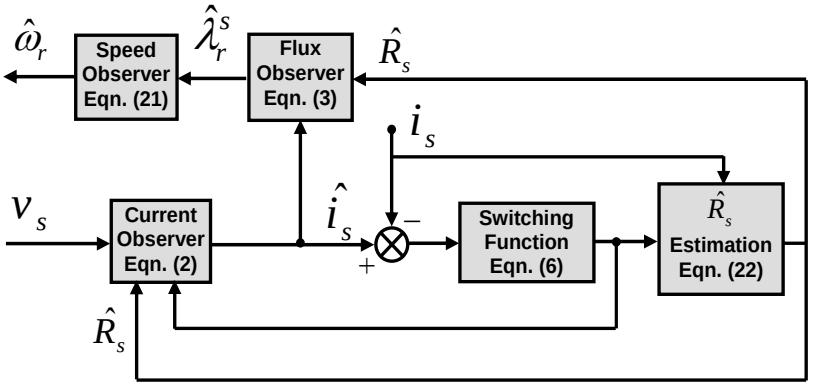

Fig. 2 Block diagram of parallel speed and stator resistance identification schemes

3. SYSTEM IMPLEMENTATION

The basic configuration of the experimental system is shown in Fig. 3. It consists of an induction motor interfaced with a digital control board DS1102 based on a Texas Instruments TMS320C31 Digital Signal Processor for speed estimation. The induction motor is coupled with a dc generator for mechanical loading. The rating and parameters of the induction motor are given in the appendix. Stator terminal voltages and currents are measured and filtered using analogue circuitry. Hall-effect sensors are used for this purpose. Measurements are taken on two phases only and the corresponding values of the third phase are obtained by calculation. The measured voltage and current signals are acquired by the A/D input ports of the DSP control board. This board is hosted by a personal computer on which mathematical algorithms are programmed and downloaded to

the board for real-time speed estimation. A direct speed measurement is also carried out for comparison with estimated speed signals. The output switching commands of the DSP control board are obtained via its digital port and interfaced with the inverter through opto-isolated gate drive circuits.

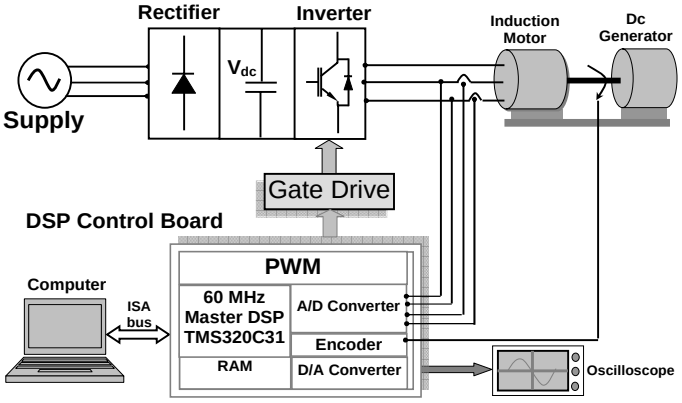

Fig. 3 Block diagram of the experimental system

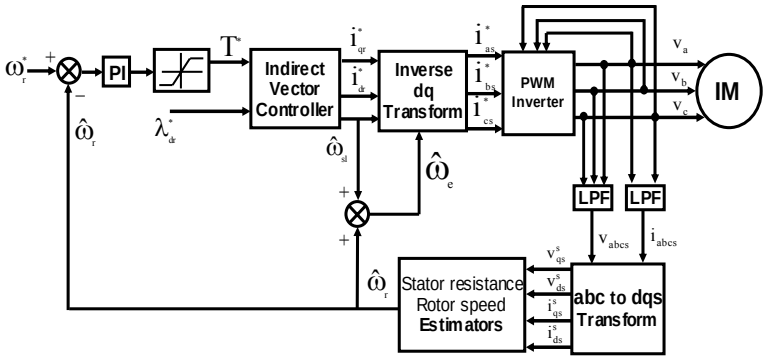

Fig. 4 Block diagram of sensorless indirect field oriented control System

4. RESULTS AND DISCUSSION

4.1. SIMULATION RESULTS

A sensorless indirect field oriented controlled induction motor drive, shown in Fig. 4, is used where the actual speed feedback signal is replaced by the estimated one. The sensitivity to stator resistance mismatch is shown in Fig. 5 for +20% R_s error at high and low speeds. These results show that, the speed estimation error at high speed operation is 1.9 rad/sec (1.26%) and at low speed operation is 0.32 rad/sec (10.7%). Large error at low speed may cause instability at low speeds. In order to avoid this, the online stator resistance adaptation scheme (22) has been applied. The initial detuning in the stator resistance takes values of -10% and -50% as shown in Fig. 6 In both cases, the stator resistance adaptation was activated at t= 0. It is clear that the stator resistance estimator quickly removes the initial stator resistance error. The stator resistance identification scheme is used in parallel with the speed estimation algorithm. The drive system is operated initially with a detuned stator resistance at a certain steady state condition and the stator resistance identification scheme is then turned on at t = 1 sec. Figure 7 shows the actual and estimated speeds as well as the speed estimation error for two initial levels of stator resistance mismatch at a speed reference of 2 rad/sec under no load condition. The initial detuning in the stator resistance is +50% and +30%, respectively. Stator resistance adaptation scheme is turned

on at t = 1 sec. It is clear from this figure that activation of the stator resistance adaptation scheme quickly compensates for the initial error in the estimated stator resistance value and, therefore, eliminates the initial speed estimation error.

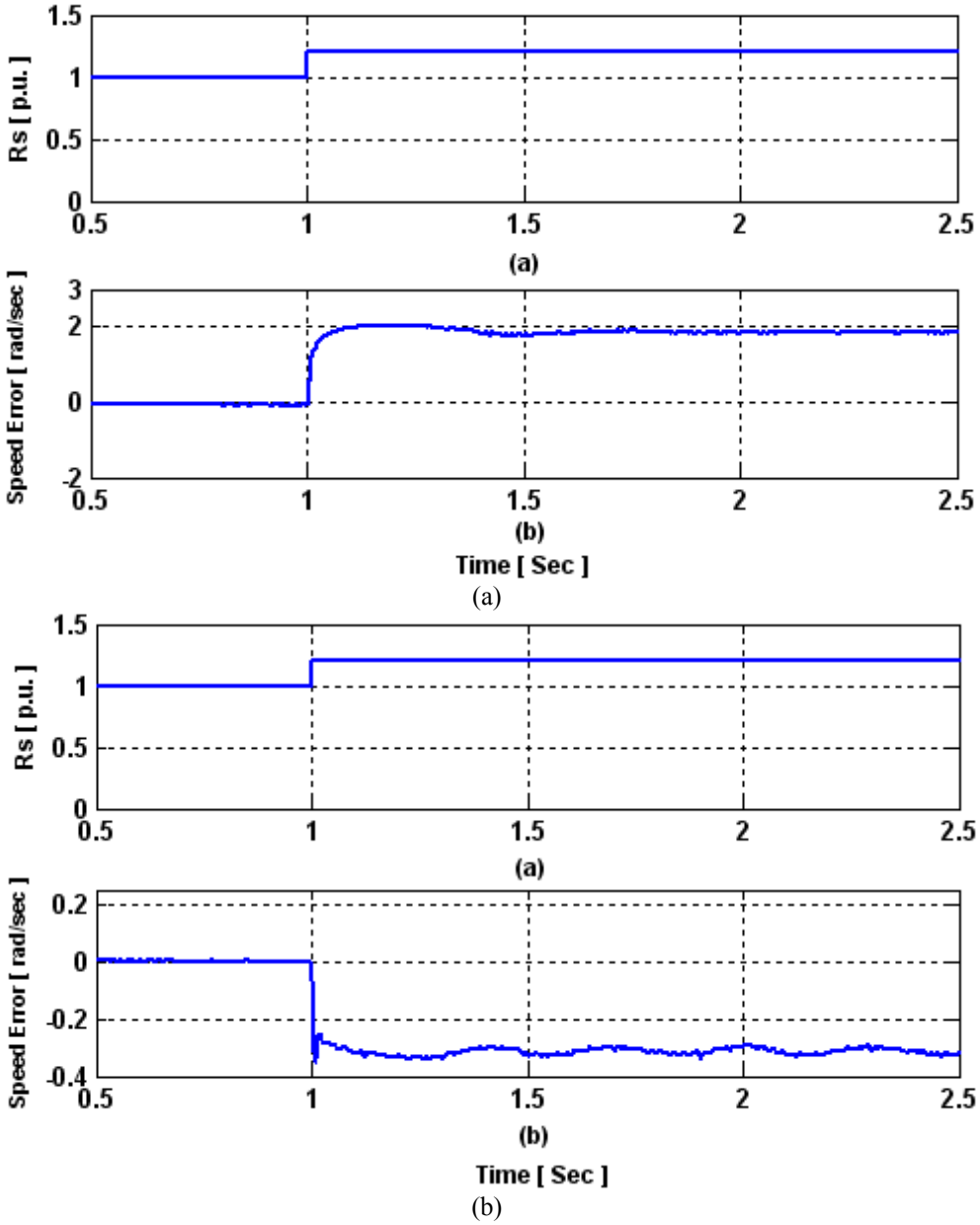

Fig.5 Speed estimation error for +20% R_s error in the observer at (a) 150 rad/sec and (b) 3 rad/sec

The same simulation results are obtained at speed reference equals 1 rad/sec under no load condition as shown in Fig. 8 with + 30% initial detuning in the stator resistance. There exists a substantial speed estimation error between the actual and estimated speeds. The stator resistance adaptation scheme is turned on at t = 1 sec. In all cases, stator resistance

estimator quickly removes the initial stator resistance error, enabling complete elimination of the speed estimation error as observed clearly from Fig. 8.

The speed observer with parallel online stator resistance identification is also examined during starting operation in the low speed region. Fig. 9 shows the actual and estimated speeds, and the speed estimation error with speed reference set at 2 rad/sec and 1 rad/sec respectively, under no load condition. It is observed that good speed estimation is achieved and the speed estimation error rapidly decays to zero.

The performance of identification schemes is also tested during speed reversal in the low speed region. Fig. 10 illustrates the actual and estimated speeds as well as the speed estimation error during speed reversal from 2 to -2 rad/sec, while, Fig. 11 shows the actual and estimated speeds and the speed estimation error during speed reversal from 1 to -1 rad/sec. Speed reversal from 0.5 to -0.5 rad/sec is also shown in Fig.12. The correct value of the stator resistance leads to elimination of the speed estimation error and the actual and estimated speeds are in very good agreement in steady state with a considerable reduction of the speed error (12.5%) during transients to zero in 0.25 sec.

The speed observer is able to operate at zero speed, provided that the estimated stator resistance exactly matches the actual stator resistance. Figure 13 shows the actual and estimated speeds as well as the speed estimation error at zero speed with stator resistance tuning. As shown, the proposed speed observer with stator resistance adaptation achieves good speed estimation. Furthermore, the results confirm that due to the accurate stator resistance estimation, the drive does not loose stability during operation at low speeds. Finally, simulation results prove the supremacy of the parallel speed and stator resistance identification schemes to provide an accurate speed estimate in the very low speed region and at zero speed.

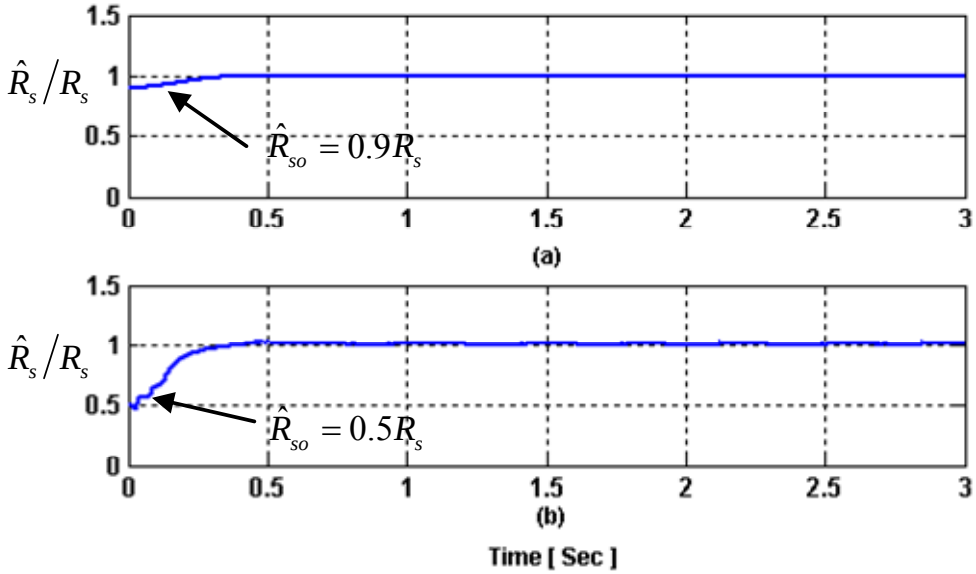

Fig.6 stator resistance adaptation for -10% and -50% R_s initial detuning at 150 rad/sec

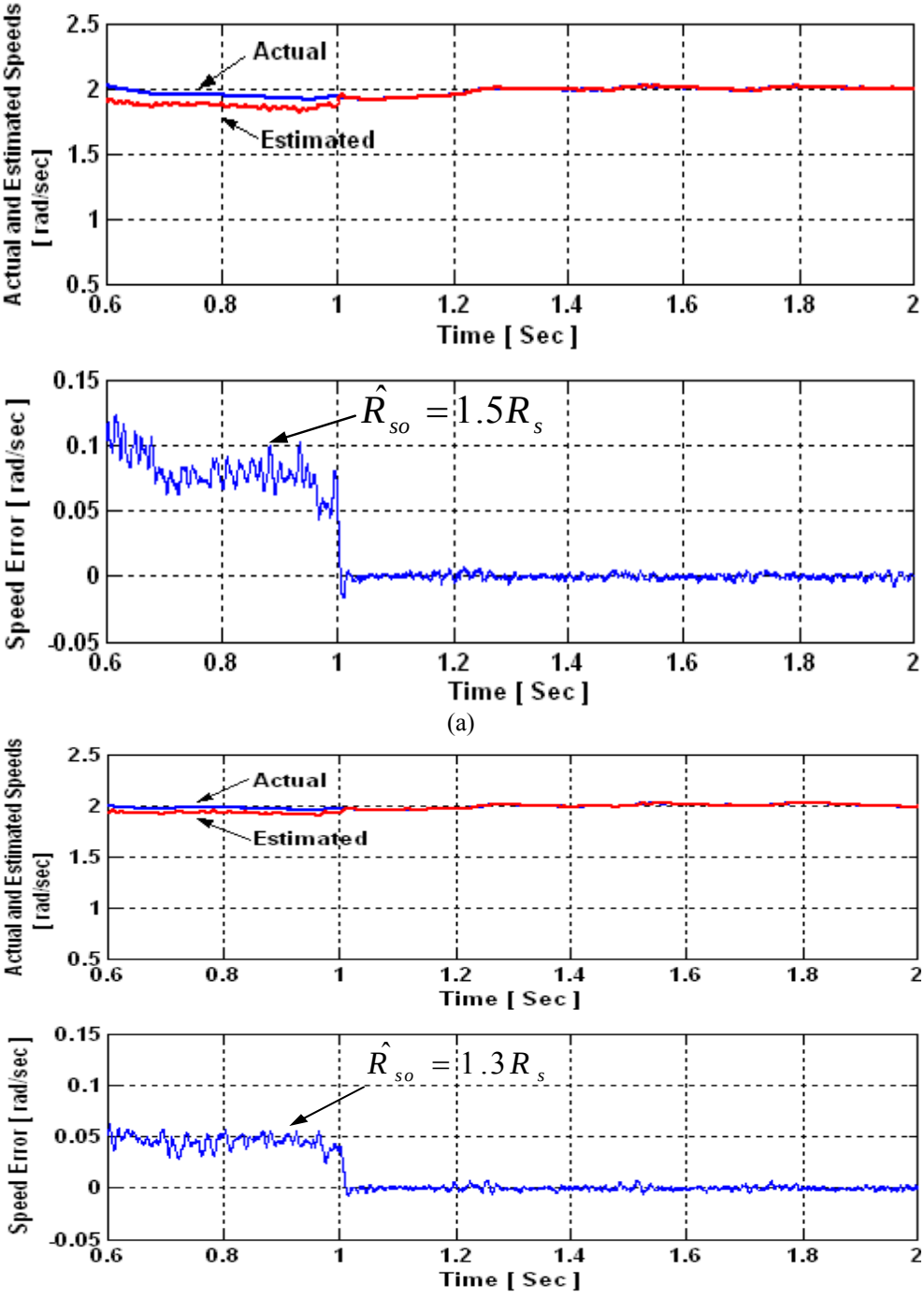

Fig. 7 Actual and estimated speeds, and speed estimation error at speed command of 2 rad/sec. Stator resistance adaptation is activated at *t = 1 sec*. (a) $\hat{R}_{so} = 1.5R_s$ and (b) $\hat{R}_{so} = 1.3R_s$

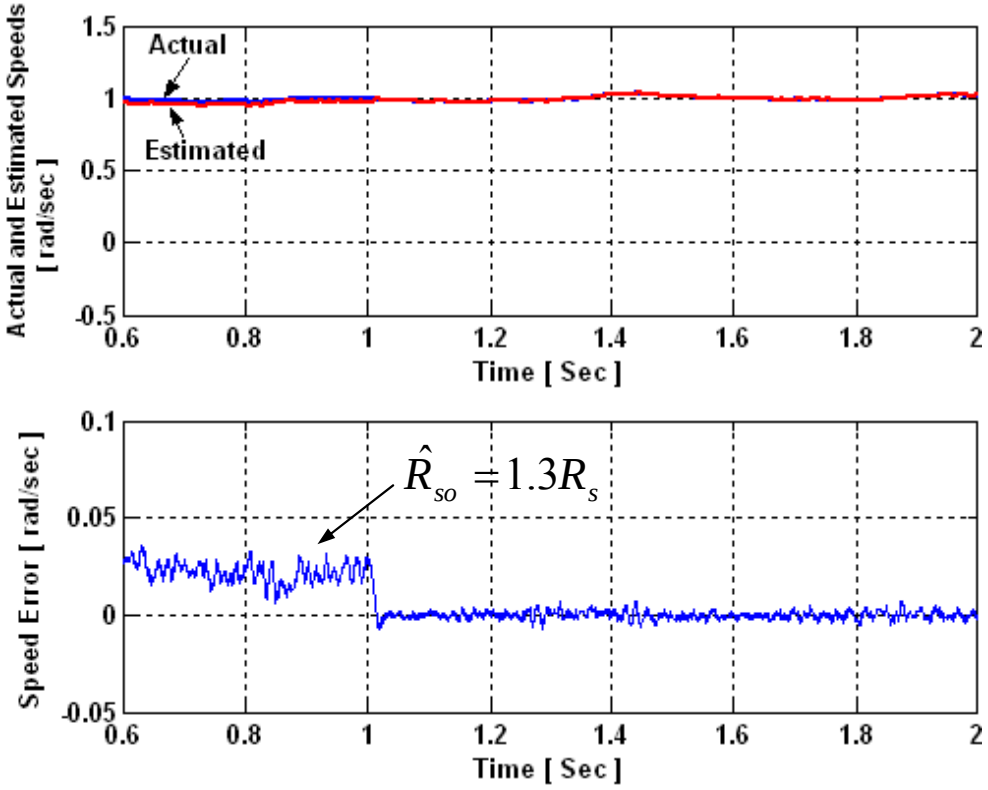

Fig. 8 Actual and estimated speeds, and speed estimation error at speed command of 1 rad/sec. Stator resistance adaptation is activated at *t = 1 sec*. $\hat{R}_{so} = 1.3R_s$

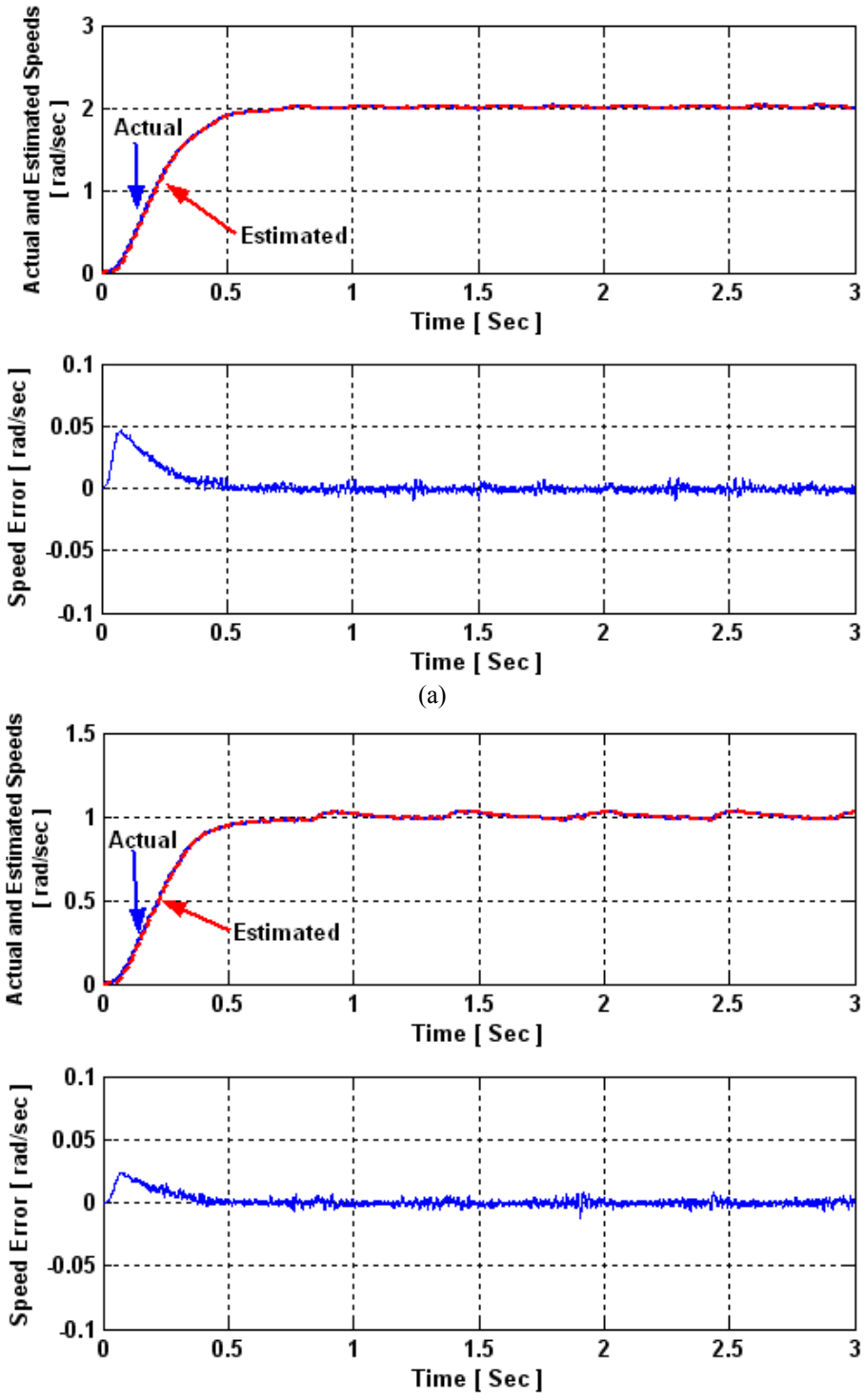

Fig. 9 Actual and estimated speeds, and speed estimation error during starting operation with stator resistance tuning at speed commands of (a) 2 rad/sec and (b) 1 rad/sec

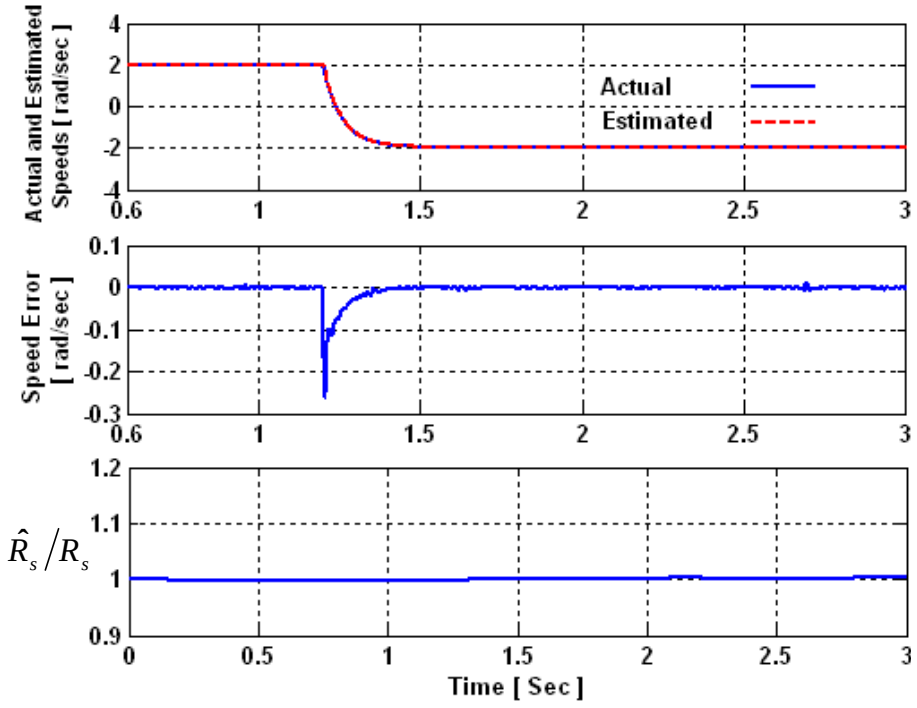

Fig. 10 Actual and estimated speeds, and speed estimation error with stator resistance tuning during speed reversal from 2 to -2 rad/sec

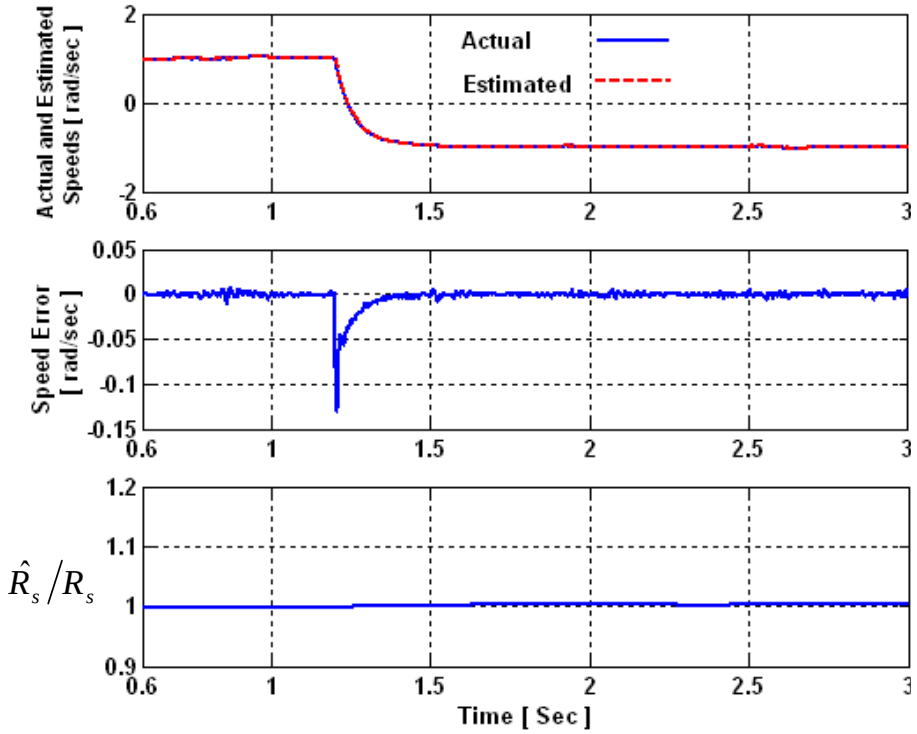

Fig. 11 Actual and estimated speeds, and speed estimation error with stator resistance tuning during speed reversal from 1 to -1 rad/sec

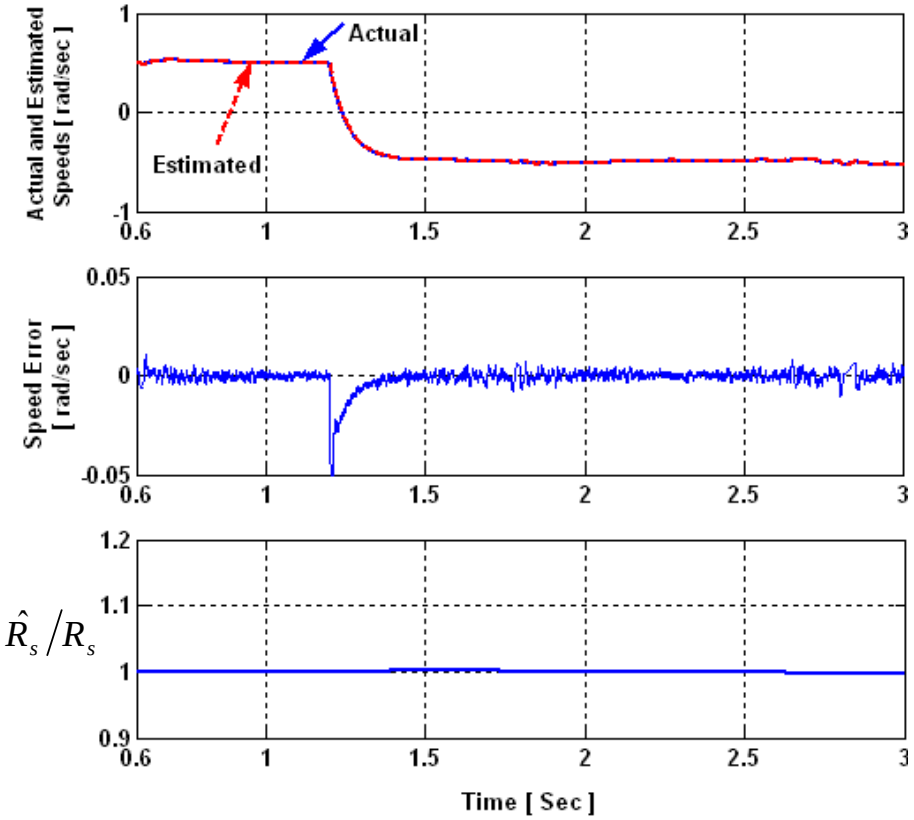

Fig. 12 Actual and estimated speeds, and speed estimation error with stator resistance tuning during speed reversal from 0.5 to -0.5 rad/sec

4.2. EXPERIMENTAL RESULTS

Since motor heating usually causes a considerable variation in the winding resistance, so there is often a mismatch between the actual stator resistance and its corresponding set value within the model used for speed estimation. Experimental results are presented to verify the performance of the proposed speed observer with stator resistance identification scheme. It is important to use a stator resistance adaptation algorithm to set an accurate value of stator resistance to the speed observer and always track the exact stator resistance and consequently a good speed estimation is achieved. Also, stator resistance adaptation mechanism makes the speed estimation algorithm robust to this parameter mismatch. For this purpose, the proposed SMO with stator resistance identification scheme is firstly tested under different values of stator resistance to represent this parameter mismatch. Fig. 14 shows the estimated speed at 10 rad/sec at +50% stator resistance mismatch with activated stator resistance adaptation. It is observed that the estimated speed preserves its value unchanged under this parameter mismatch. This test proves that the proposed SMO with online stator resistance tuning is dependable and accurately gives the same behavior as the actual speed under stator resistance mismatch.

The effectiveness of stator resistance adaptation algorithm is tested during reversing transients, this corresponds to a very short-term operation at zero speed. Figure 15 shows the actual and estimated speeds for a reversing transient from 100 to -100 rad/sec with and without stator resistance adaptation.

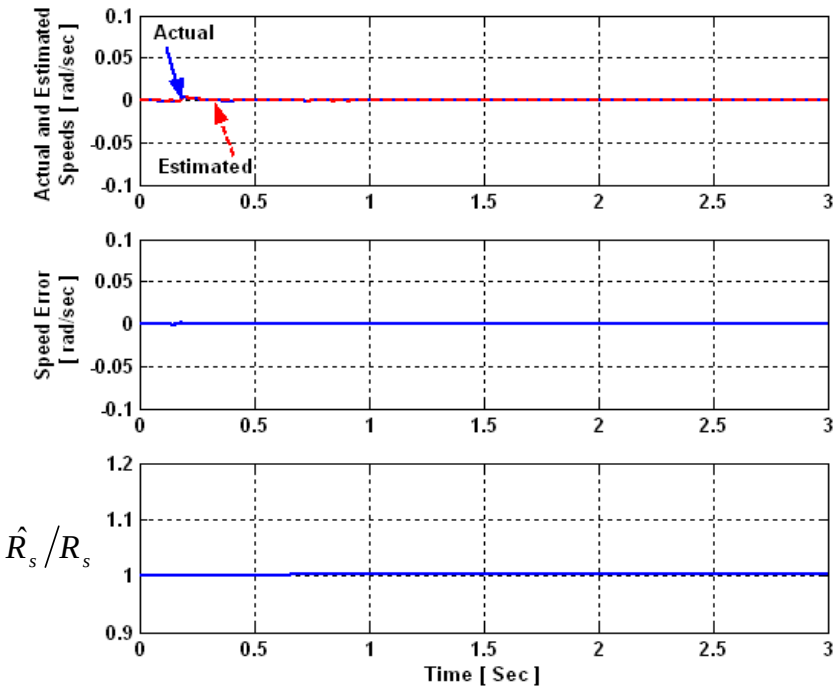

Fig. 13 Actual and estimated speeds, and speed estimation error with stator resistance tuning at zero speed

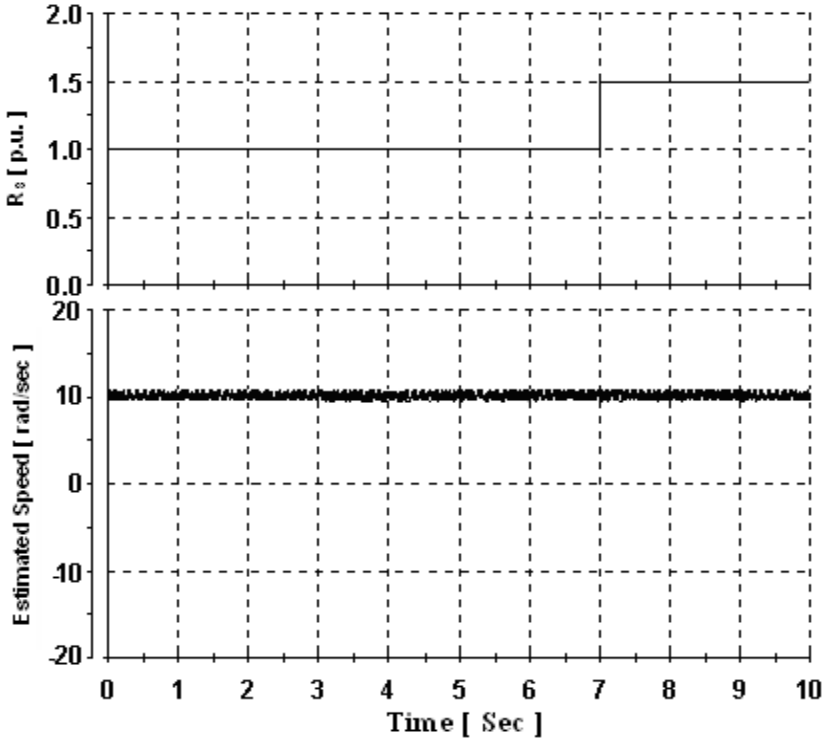

Fig. 14 Estimated speed at 10 rad/sec under +50% mismatch of stator resistance with stator resistance adaptation

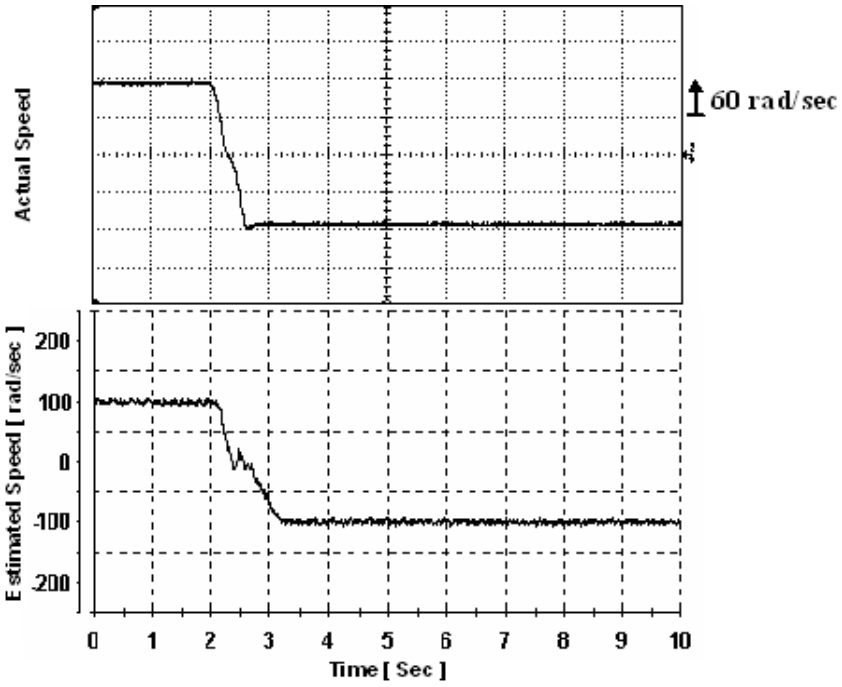

(a)

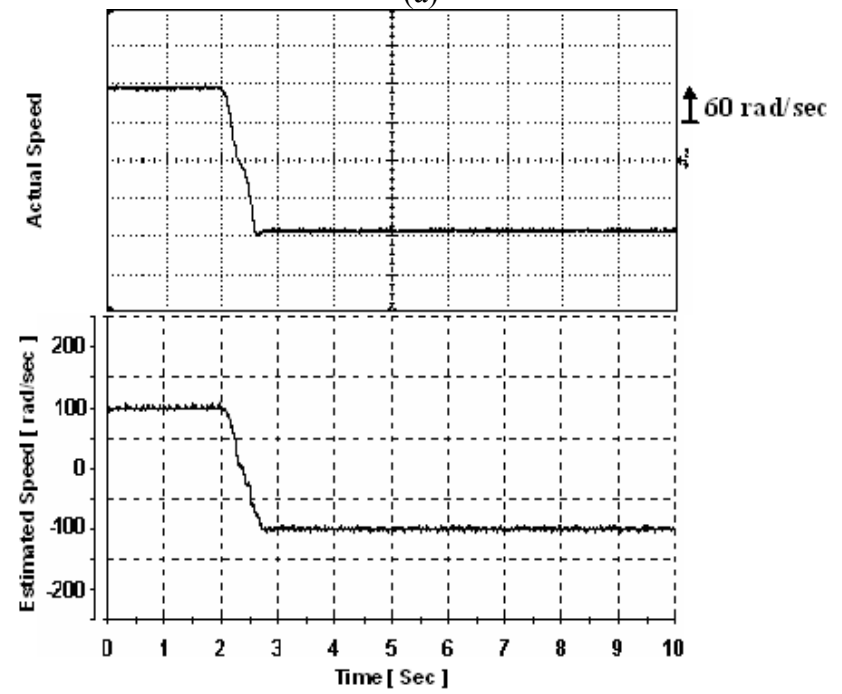

(b)

Fig. 15 Actual and estimated speed during speed reversal at 100 rad/sec (a) without stator resistance adaptation and (b) with stator resistance adaptation

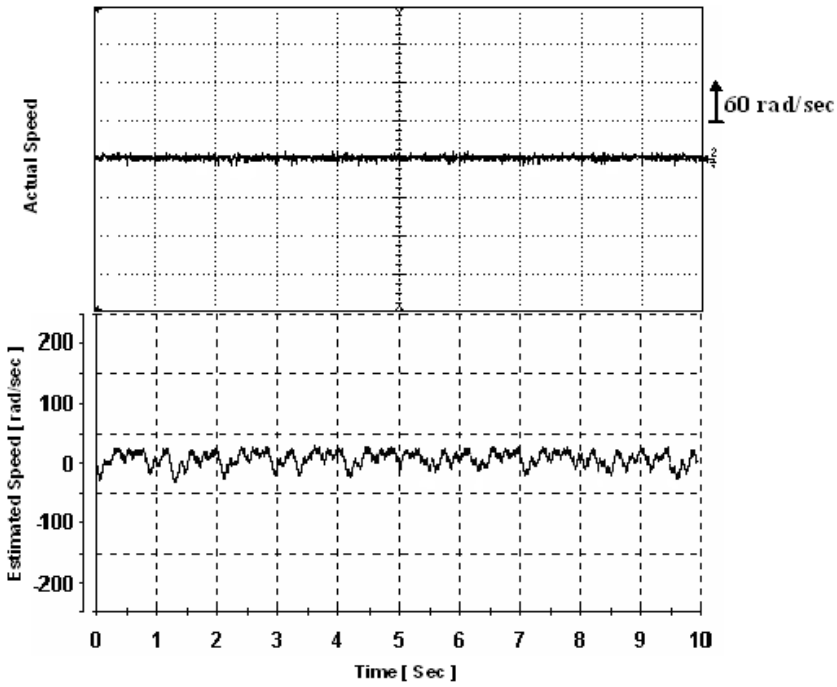

(a)

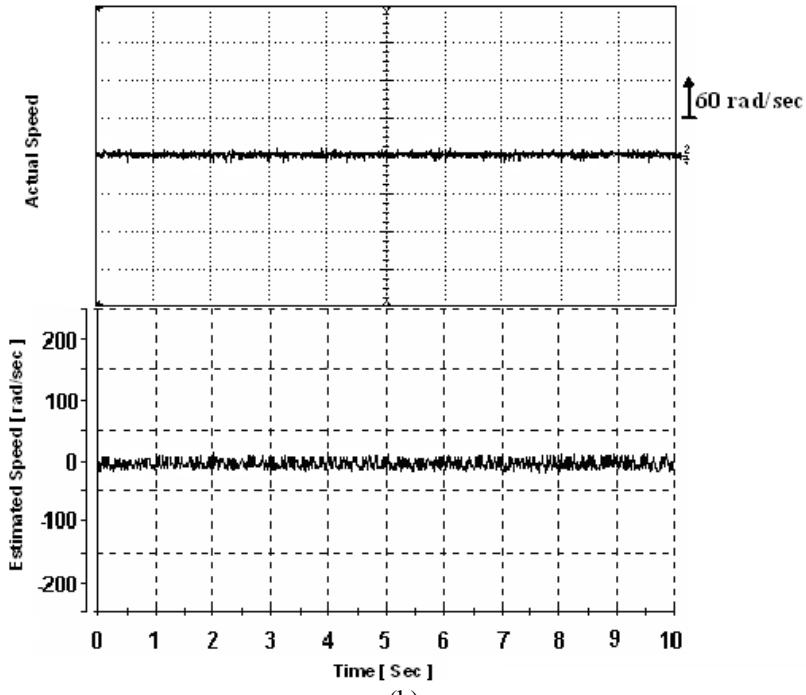

(b)

Fig. 16 Actual and estimated speed at zero speed (a) without stator resistance adaptation and (b) with stator resistance adaptation

The results with stator resistance adaptation mechanism illustrate that good estimated speed during reversing transient through zero speed is achieved compared with the same situation in Fig. 15-b. Persistent operation at zero speed is possible experimentally as shown in Fig. 16 with and without stator resistance adaptation. Figure 17 shows the actual and estimated speeds for a reversing transient from 60 to -60 rad/sec with stator resistance adaptation. The stator resistance identification scheme is also examined at very low speeds. Figure 18 shows the experimental results during steady state operation at 2.5 rad/sec (0.8 Hz, 0.016 p.u.). This figure shows good speed estimation due to the introduction of stator resistance adaptation.

The introduced results demonstrate that the system exhibits a good robustness and high speed estimation accuracy under different operating conditions and with stator resistance mismatch. This is possible due to the strong robustness of the SMO.

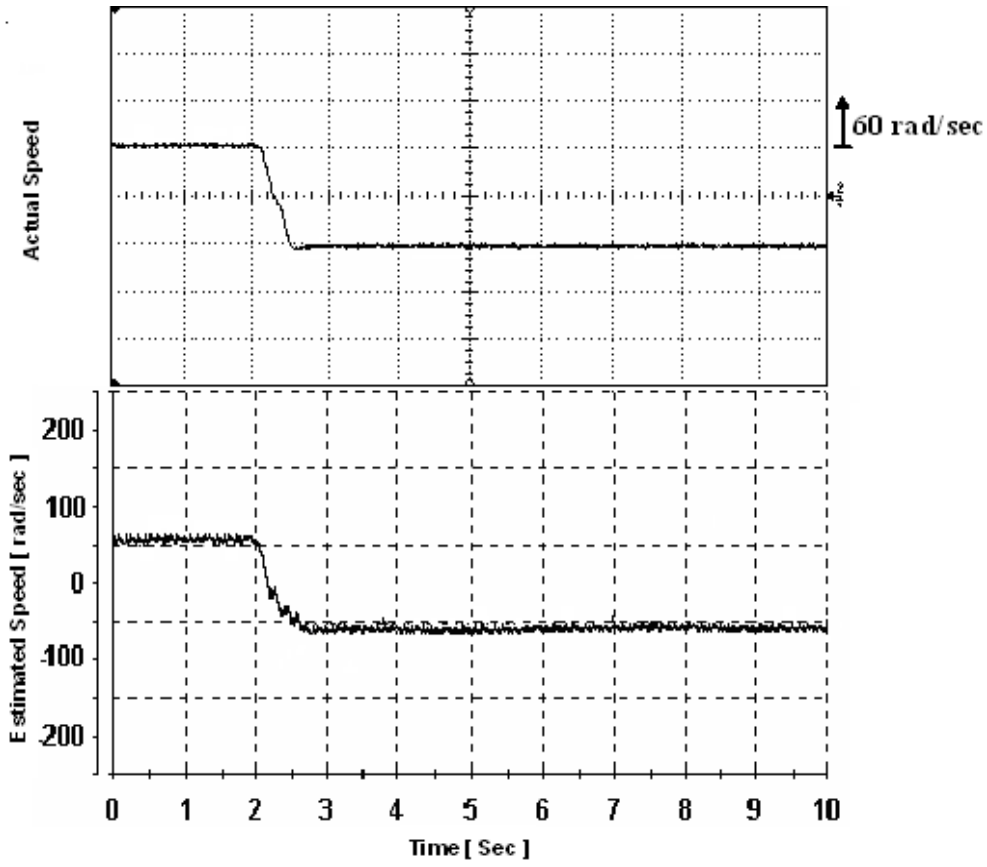

Fig. 17 Actual and estimated speed during speed reversal at 60 rad/sec with stator resistance adaptation

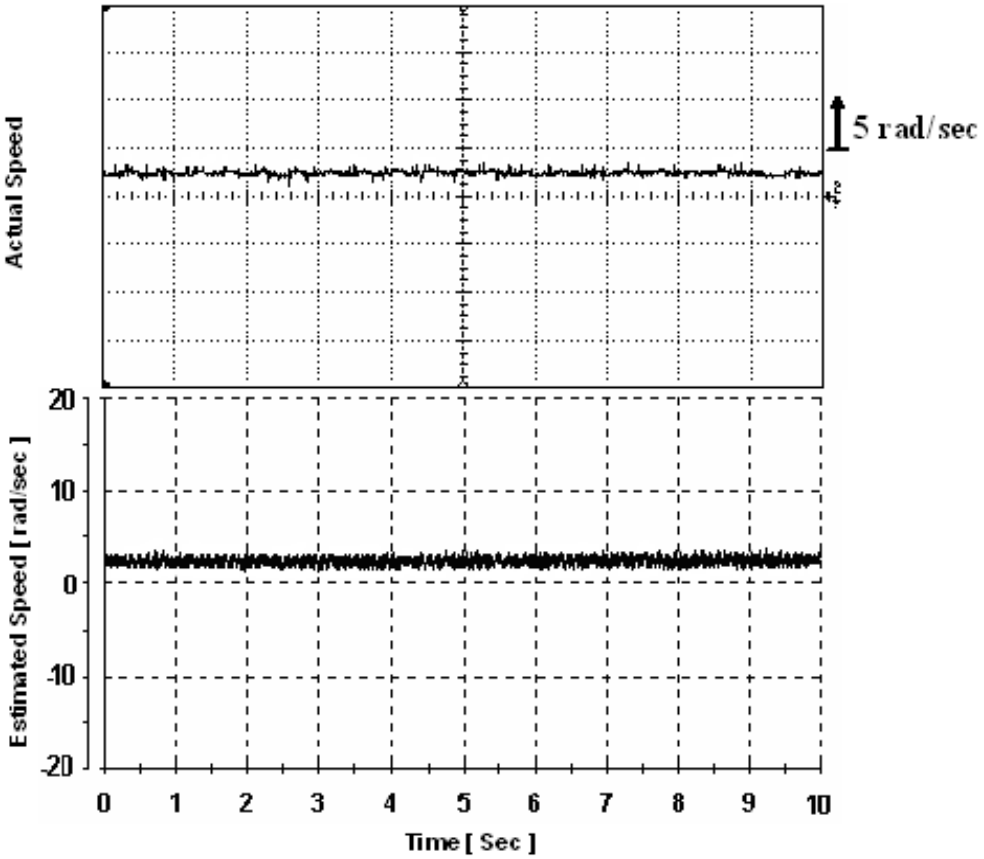

Fig. 18 Actual and estimated speed during steady state operation at 2.5 rad/sec (0.8 Hz, 0.016 p.u.) with stator resistance adaptation

5. CONCLUSION

In this paper, a parallel speed and stator resistance identification schemes of sensorless induction motor drives have been presented. The estimation algorithms have been obtained based on sliding mode current observer combined with Lyapunov stability and Popov's hyper-stability theories which are applied to nonlinear feedback systems. It has been found that activation of the stator resistance adaptation mechanism quickly compensates the initial error in the estimated stator resistance value and, therefore, eliminates the initial speed estimation error. As a consequence, the actual and estimated speeds are in good agreement. Very low speed sensorless operation and also zero speed have been investigated by the proposed SMO with online stator resistance adaptation scheme. Extensive simulation results have been presented to prove the supremacy of the proposed system, and experimental results using DSP are included as well.

References

[1] M. S. Zaky, M. M. Khater, H. Yasin, and S. S. Shokralla, A. El-Sabbe, " Speed-sensorless control of induction motor drives (Review Paper)", Engineering Research Journal (ERJ), Faculty of Engineering, Minoufiya University, Egypt, Vol. 30, No. 4, October 2007, PP. 433-444.

[2] M. S. Zaky, M. M. Khater, H. Yasin, and S. S. Shokralla, A. El-Sabbe, " Robust sliding mode speed observer for induction motor drives", Engineering Research Journal (ERJ), Faculty of Engineering, Minoufiya University, Egypt, Vol. 30, No. 4, October 2007, PP. 425-431.

[3] Hirokazu Tajima, Giuseppe Guidi, and Hidetoshi Umida, "Consideration about problems and solutions of speed estimation method and parameter tuning for speed-sensorless vector control of induction motor drives," IEEE Trans. on Ind. Applicat., Vol. 38, No. 5, September/October 2002, pp. 1282-1289.

[4] Joachim Holtz, and Juntao Quan, "Sensorless vector control of induction motors at very low speed using a nonlinear inverter model and parameter identification," IEEE Trans. on Ind. Applicat., Vol. 38, NO. 4, July/August 2002, pp. 1087-1095.

[5] Giuseppe Guidi, and Hidetoshi Umida, "A Novel Stator Resistance Estimation Method for Speed-Sensorless Induction Motor Drives," IEEE Transactions on Industry Applications, Vol. 36, NO. 6, November/December 2000, pp. 1619-1627.

[6] Gregor Edelbaher, Karel Jezernik, and Evgen Urlep, "Low-speed sensorless control of induction machine," IEEE Trans. on Ind. Electr., Vol. 53, No. 1, February 2006, PP. 120-129.

[7] Hossein Madadi Kojabadia, and Liuchen Changb, "Comparative study of pole placement methods in adaptive flux observers," Control Engineering Practice, Elsevier, Vol. 13, 2005, pp. 749–757.

[8] Jehudi Maes and Jan A. Melkebeek, "Speed-Sensorless direct torque control of induction motors using an adaptive flux observer," IEEE Trans. on Ind. Applicat., Vol. 36, NO. 3, May/June 2000, pp. 778-785.

[9] H. Mdaadi Kojabadi, "Simulation and experimental studies of model reference adaptive system for sensorless induction motor drive," Simulation Modeling Practice and Theory, Elsevier, Vol. 13, 2005, pp. 451–464.

[10] Veran Vasic, Slobodan N. Vukosavic, and Emil Levi, "A stator resistance estimation scheme for speed sensorless rotor flux oriented induction motor drives," IEEE Trans. on Energy Conversion, Vol. 18, No. 4, December 2003, pp. 476-483.

6. Appendix

A. List of symbols

L_m	Mutual inductance
L_r	Rotor leakage inductance
L_s	Stator leakage inductance
R_s	Stator resistance
T_r	Rotor time constant
ω_r	Rotor angular speed
σ	Leakage coefficient
$i_s^s = [i_{ds}^s \quad i_{qs}^s]^T$	Stator current vector
$\hat{i}_s^s = [\hat{i}_{ds}^s \quad \hat{i}_{qs}^s]^T$	Estimated Stator current vector
$\lambda_r^s = [\lambda_{dr}^s \quad \lambda_{qr}^s]^T$	Rotor flux vector
$\hat{\lambda}_r^s = [\hat{\lambda}_{dr}^s \quad \hat{\lambda}_{qr}^s]^T$	Estimated rotor flux vector
$v_s^s = [v_{ds}^s \quad v_{qs}^s]^T$	Stator voltage vector
$\hat{\omega}_r$	Estimated rotor speed
$p = d/dt$	Differential operator

$$A_{11} = aI, \quad A_{12} = cI + dJ, \quad A_{21} = eI, \quad A_{22} = -\varepsilon A_{12}, \quad b_1 = bI$$

$$I = \begin{bmatrix} 1 & 0 \\ 0 & 1 \end{bmatrix}, \quad J = \begin{bmatrix} 0 & -1 \\ 1 & 0 \end{bmatrix}$$

$$a = -\left(\frac{R_s}{\sigma L_s} + \frac{L_m^2}{\sigma L_s T_r L_r} \right), \quad c = \frac{1}{\varepsilon T_r}, \quad d = \frac{\omega_r}{\varepsilon}, \quad e = \frac{L_m}{T_r}$$

$$\varepsilon = \frac{\sigma L_s L_r}{L_m}, \quad b = \frac{1}{\sigma L_s}, \quad \sigma = 1 - \frac{L_m^2}{L_s L_r}, \quad T_r = \frac{L_r}{R_r}$$

B. Induction motor parameters:-

Rated power (w)	250	R_s (p.u)	0.0658
Rated voltage (volt)	380	R_r (p.u)	0.0485
Rated current (Amp.)	0.5	L_s (p.u)	0.6274
Rated frequency (Hz)	50	L_r (p.u)	0.6274
Number of poles	4	L_m (p.u)	0.5406